Polymer 81 (2015) 87–98

Contents lists available at ScienceDirect

Polymer

journal homepage: www.elsevier.com/locate/polymer

Gas transport in metal organic framework–polyetherimide mixed matrix membranes: The role of the polyetherimide backbone structure

Maruti Hegde [a, c], Salman Shahid [c], Ben Norder [b], Theo J. Dingemans [a, **], Kitty Nijmeijer [c, *]

[a] Novel Aerospace Materials, Faculty of Aerospace Engineering, Delft University of Technology, Kluyverweg 1, 2629 HS Delft, The Netherlands
[b] Advanced Soft Matter, Technische Natuurwetenschappen (TNW), Delft University of Technology, Julianalaan 136, 2628 BL Delft, The Netherlands
[c] Membrane Science and Technology, MESA+ Institute for Nanotechnology, Faculty of Science and Technology, University of Twente, Drienerlolaan 5, 7522 NB Enschede, The Netherlands

ARTICLE INFO

Article history:
Received 1 September 2015
Accepted 1 November 2015
Available online 6 November 2015

Keywords:
Mixed matrix membranes
Polyetherimide
Membrane morphology

ABSTRACT

We report on how the morphology of the polymer matrix, *i.e.* amorphous vs. semi-crystalline, affects the gas transport properties in a series of mixed matrix membranes (MMMs) using $Cu_3(BTC)_2$ as the metal organic framework (MOF) filler. The aim of our work is to demonstrate how incorporation of $Cu_3(BTC)_2$ affects the polyetherimide matrix morphology and thereby highlighting the importance of selecting the appropriate polyetherimide matrix for mixed matrix membranes.

We used three amorphous poly(etherimide)s with very similar backbone structures. Polyetherimide ODPA-P1 was used as a linear flexible matrix, aBPDA-P1 is a non-linear rigid matrix and 6FDA-P1 was selected because the backbone structure is similar to ODPA-P1 but replacing the oxygen linker with two bulky $-CF_3$ groups results in a linear polymer with a low chain packing efficiency. Using an *in-situ* polymerization technique, up to 20 wt.% $Cu_3(BTC)_2$ could be homogenously dispersed in all three PEIs. The ODPA-P1 matrix crystallized when $Cu_3(BTC)_2$ was introduced as a filler. Gas permeation studies were performed by analyzing membrane performance using a 50:50 CO_2:CH_4 mixed gas feed. The presence of crystalline domains in ODPA-P1 resulted in a decrease in permeability for both CO_2 and CH_4 but the selectivity increased from 41 to 52 at 20 wt.% $Cu_3(BTC)_2$. The non-linear, rigid, aBPDA-P1 matrix remains amorphous when $Cu_3(BTC)_2$ is introduced. SEM images of the MMM cross-section revealed a sieve-in-a-cage morphology and at 20 wt.% $Cu_3(BTC)_2$, the permeation of both CO_2 and CH_4 increased by 68% thereby negating any change in selectivity. For 6FDA-P1 with 20 wt.% $Cu_3(BTC)_2$, only the permeability of CO_2 increased by 68% resulting in an increase in selectivity of 33%.

1. Introduction

3-D crystalline metal organic frameworks (MOFs) combined with polymeric matrices are prime candidates for separating gas mixtures [1]. The MOF filler contributes tunable chemistry [2,3], large surface area [4–6], adjustable pore size [7], selective affinity towards gas molecules [8–10], and high thermal stability [11]. These attributes make them attractive as additives for improving gas permeability and selectivity of polymeric membranes.

Although the gas separation properties of composite materials using inorganic fillers such as zeolites or sieves in a polymer matrix have been researched extensively, gas separation in polymer–MOF composites is less well understood [12,13]. So far, it is known that the low affinity of the polymer towards the inorganic filler generally results in the formation of non-selective voids at the polymer–filler interface, which in turn degrades the gas transport performance of the membrane [14]. Evidence of poor wetting by the polymer and debonding of the filler has been presented in scanning electron microscopy (SEM) images of membrane cross-sections [15]. In mixed matrix membranes (MMMs) using MOFs as fillers, the presence of organic ligands in MOFs is expected to

* Corresponding author.
** Corresponding author.
E-mail addresses: t.j.dingemans@tudelft.nl (T.J. Dingemans), d.c.nijmeijer@utwente.nl (K. Nijmeijer).

http://dx.doi.org/10.1016/j.polymer.2015.11.002
0032-3861/

lead to 'better' interfaces with the polymer matrix and therefore improve gas permeability and selectivity. Recent publications from our group and others have shown that increments in gas transport are indeed possible when modifying polymer matrices with MOFs [8,16,17,18,19]. But often, only an increase in permeability of the MMMs was observed without any increase in gas selectivity [6,20,21]. In general, the incorporation of MOFs in rubbery polymers leads to defect free MMMs but the high permeability of such polymers diminishes the contribution of the MOF fillers to gas transport [22,23]. In comparison, the use of high glass transition (Tg) rigid aromatic polyimides such as Matrimid® results in MMMs with a large number of non-selective voids at the interface [24,25]. Consequently, only an increase in gas permeability is obtained without any corresponding increase in selectivity.

Most research attention in the field of MOF–polymer membranes has focused on chemical modification and functionalization of the MOFs themselves in the hope of achieving higher affinities to specific gas molecules [10,26,27,28]. A systematic and detailed investigation into molecular aspects of the polymer matrix and subsequent changes in polymer morphology due to MOF inclusion has been noticeably absent. It must be noted that there have been some important contributions towards understanding polymer chain organization in the presence of zeolites such as the report published in 2004 by the group of Koros [14].

The most commonly found examples of polyimide matrices in literature are based on Matrimid™, P84, 6FDA-ODA and Ultem™. These matrices are known to have excellent gas-separation properties and they are solution processable. The lack of solubility of aromatic polyimides in common solvents is a reason for the commonly utilized two-step approach towards their synthesis. The first step involves preparing a solution of the soluble polyamic-acid intermediate. This polyamic acid is then cast as a film, the solvent is removed under vacuum at 60 °C and then subsequently the film is thermally imidized in steps up to 300 °C to form the insoluble polyimide. If the MOFs could be distributed homogenously in the polyamic-acid intermediate and the 3-D structure of the MOF could be maintained during thermal imidization, the field could be opened for a host of polyimide matrices that otherwise cannot be utilized.

Most reported mixed matrix membranes so far have been prepared using $Cu_3(BTC)_2$. The MOF $Cu_3(BTC)_2$ has a rigid 3D cubic structure with a main central cage having dimensions between 1 and 1.2 nm and intersectional pores with 0.6 nm tetrahedral side pockets. The main central cage and tetrahedral side pockets are connected by triangular windows of 0.35 nm that enable size sieving of gas molecules [18]. $Cu_3(BTC)_2$ has also been reported to exhibit a high affinity towards CO_2, which makes it attractive in separating CO_2 from CH_4 in natural gas feeds [29,30].

In terms of choosing polymer structures as the matrix, we have selected three poly(etherimide)s based on one all-aromatic diamine (1,4-bis(4-aminophenoxy) benzene, labeled **P1**) and 3 different dianhydrides (Scheme 1).

The ODPA-P1 polymer is an amorphous high performance all-aromatic polyetherimide that has been previously reported in literature [31]. In comparison to the other two polymers, this polymer is the most linear and most flexible and is anticipated to exhibit the highest chain packing density. In a past publication by Simons et al., the selectivity of CO_2 over CH_4 was reported to be ~50 at 5 bars for amorphous ODPA-P1 [32]. The linearity and conformational flexibility of this polymer is reflected in its ability to form crystal domains when cast and thermally imidized from polyamic acid solutions at concentrations of 10 wt.% or lower in NMP [33]. This makes it an ideal polymer matrix as it allows us to study the morphological changes induced by MOF inclusion and the subsequent changes in gas transport properties.

In contrast to ODPA-P1, 2,3′,3,4′-biphenyltetracarboxylic dianhydride or asymmetric BPDA and P1 (aBPDA-P1) results in a highly kinked and rigid polymer due to the asymmetry of the dianhydride moiety. The inability of this polymer to undergo crankshaft rotations around the C–C bond of the phenyl groups in aBPDA renders this polymer very rigid [34]. As far as we know, this polyetherimide has not been reported in the literature.

The incorporation of hexafluoroisopropylidene $(-CF_3)_2$ groups into the polymer backbone, as is the case for 6FDA-P1 (Scheme 1), restricts intra-segmental and inter-segmental mobility [35]. Also, the presence of hexafluoroisopropylidene bulky groups hinders effective chain packing leading to low polyetherimide densities [36]. In comparison to ODPA-P1, 6FDA-P1 has a larger free volume and higher conformational rigidity but is more linear than the highly kinked aBPDA-P1. Additionally, the presence of $-CF_3$ groups have been shown to help increase selective transport of gas molecules such as CO_2 [37] and interact (non-covalent) with the MOF filler [38].

In this research article, we will report on the thermo-mechanical and gas separation properties of three $Cu_3(BTC)_2$ modified polyetherimide model systems. Using a traditional 2-step polyetherimide synthetic procedure, we explored whether the addition of MOFs at the polyamic stage of synthesis is a viable alternative to using solutions of fully imidized polyimides. This synthetic method, if successful, will open up a wide range of otherwise insoluble aromatic polyimide matrix materials. The three poly(etherimide)s selected will aid in understanding the role of polymer morphology on gas permeation and gas separation when designing mixed matrix membranes.

2. Experimental

2.1. Materials

99.9% pure 3,3′,4,4′-oxydiphthalic dianhydride (ODPA) (99.9%) was purchased from TCI Chemical Industry Co. Ltd. 99.9% pure 4,4'-Hexafluoroisopropylidenebisphthalic dianhydride (6FDA) was purchased from Akron Polymer Systems. 95.0% pure 1,4-Bis(4-aminophenoxy) benzene (P1) was purchased from ABCR Inc. 2,3′,3,4′-Biphenyltetracarboxylic dianhydride (aBPDA) (99.9%) was generously donated by UBE Inc. Dry N-Methyl-2-pyrrolidone (NMP) (water content < 0.005%) was purchased from Acros Organics and used as received. Activated $Cu_3(BTC)_2$ MOF (also known as Basolite 300) was purchased from Sigma Aldrich and used as received.

2.2. Polyetherimide synthesis

The neat poly(etherimide)s based on ODPA-P1, 6FDA-P1 and aBPDA-P1 were synthesized using a standard two-step procedure *i.e.* synthesis of the polyamic acid followed by thermal imidization. The synthesis of ODPA-P1 is shown as an example in Scheme 2 [31].

A representative synthetic procedure is as follows: Synthesis of the ODPA-P1 polyamic acid. A 50 ml single neck flask fitted with an Argon inlet was charged with 0.747 g (2.55 mmol) of 1,4-bis (4-aminophenoxy)benzene (P1) and 5 ml of dry NMP. The mixture was stirred under argon atmosphere until all the diamine monomer dissolved. The polymerization was initiated by adding 0.793 g (2.55 mmol) of 3,3′,4,4'-oxydiphthalic dianhydride (ODPA). The concentration of monomers in NMP for all polyamic acid intermediates was 22 wt.% in NMP. The solution was left to stir overnight for polymerization to be complete. Prior to film casting, all polyamic acid solutions were diluted to monomer concentration of 18 wt.% of NMP.

Synthesis of 20 wt.% $Cu_3(BTC)_2$ ODPA-P1 polyamic acid

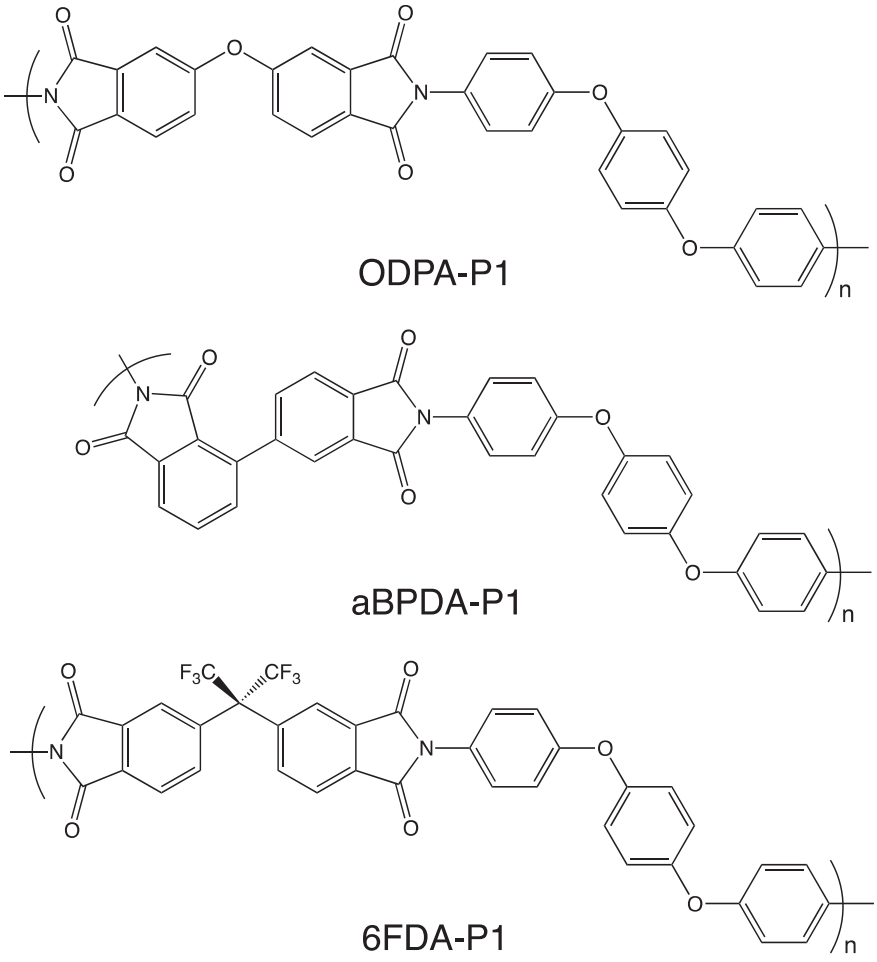

Scheme 1. Molecular structures of the polyetherimide matrices used in this study.

intermediate. 0.308 g of activated dark blue $Cu_3(BTC)_2$ MOFs was weighed in a glove box purged overnight with dry N_2. The weighed $Cu_3(BTC)_2$ powder was added to 1.5 ml of NMP in a 25 ml glass vial. The glass vial was sealed with a rubber seal before removal from the glove box. An argon needle was inserted into the glass vial and the solution bath sonicated for 20 min to achieve homogenous distribution of $Cu_3(BTC)_2$ in NMP. This solution was quickly transferred to a round-bottom flask containing 7 ml of ODPA-P1 polyamic-acid intermediate at 22 wt.% monomer concentration. The mixture now containing 18 wt.% solids was stirred under Argon for 1 h.

Thermal imidization of the polyamic acid intermediates. The solutions of polyamic acid were doctored onto a glass plate and placed in a vacuum oven purged with Argon. The NMP was removed by heating the films at 60 °C for 1.5 h under vacuum. Thermal imidization of the polyamic films was achieved by heating the films at 100 °C, 200 °C and 220 °C for 1 h each. Finally, the films on the glass plates were allowed to cool to 25 °C overnight. Good quality, tack-free, ductile films could be obtained by placing the glass plates in warm water for ~30 min.

2.3. Analysis

GPC measurements were performed using a Shimadzu GPC LC-20AD equipped with a Shodex LF-801 column and a refractive index detector using NMP containing 0.5 mmol/L LiBr as the eluent; polystyrene standards were used to calibrate the instrument. All polyamic acid intermediate solutions (prepared at concentrations of ~0.5 mg/ml) were filtered through a 0.45 μm PTFE filter prior to a GPC run.

FT-IR measurements were performed on all MMMs using a Perkin–Elmer 100 spectrometer in attenuated total reflection (ATR) mode. A constant force was applied to all samples prior to measurements and the background contribution was measured and subtracted automatically from the membrane spectra by the software. The membranes were scanned in the wavelength range between 2500 cm^{-1} and 500 cm^{-1}. An average of 25 scans were recorded per membrane.

A Nikon digital micrometer with an accuracy of 1 μm was used to measure the thickness of the films. The instrument was calibrated using three films of known thickness.

The thermal stability of the membranes was measured using a Perkin Elmer Thermo-gravimetric analyzer (TG-DTA). $Cu_3(BTC)_2$ powder (~2 mg) and mixed matrix membranes (~5 mg) were heated from 25 °C to 600 °C in aluminum sample pans at a rate of 10 °C/min in nitrogen atmosphere.

The thermal properties of the imidized membranes were determined by differential scanning calorimetry (DSC) using a Perkin–Elmer Sapphire DSC. Samples were heated at a rate of 20 °C/min under a nitrogen atmosphere from 25 °C to 320 °C. Dynamic mechanical thermal analysis (DMTA) was performed with a Perkin–Elmer Diamond DMTA. DMTA experiments on the films were performed at a frequency of 1 Hz at a heating rate of 2.0 °C/min using films having approximate dimensions of

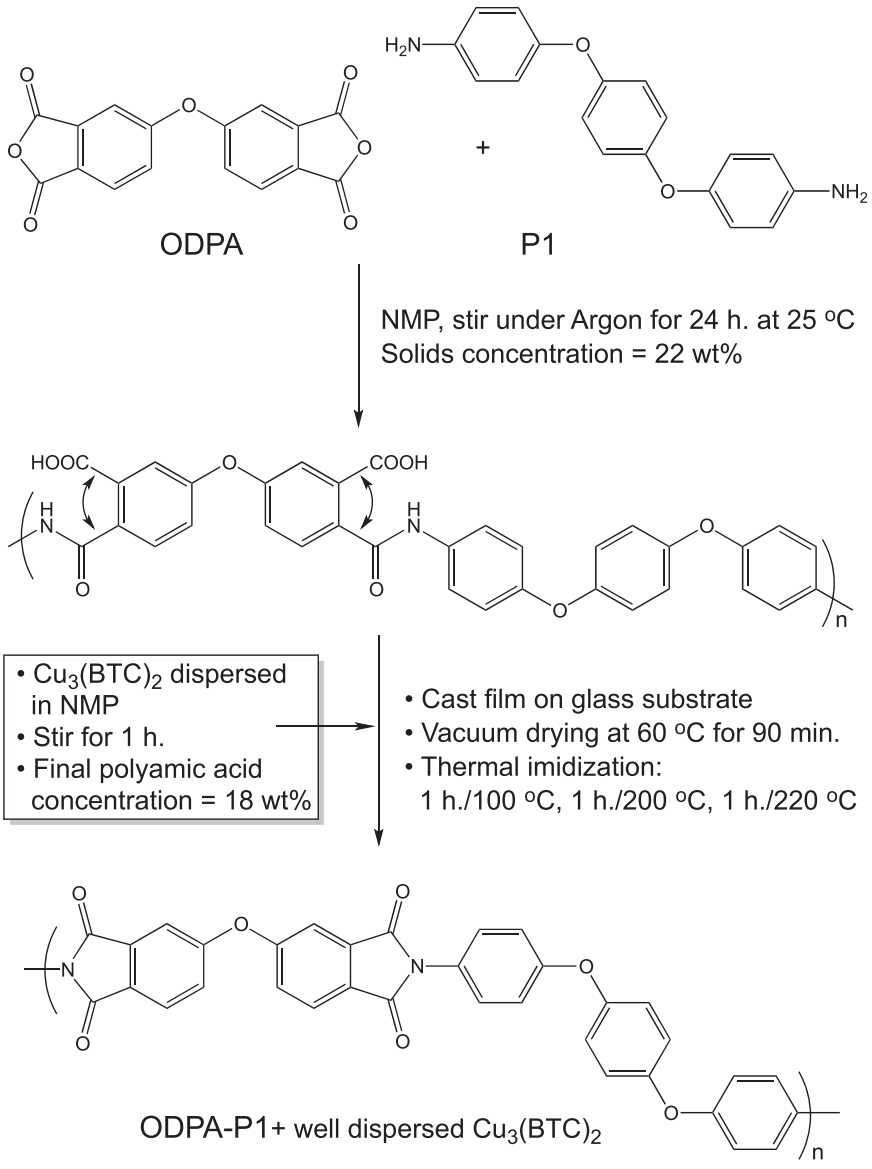

Scheme 2. Synthesis of ODPA-P1 mixed matrix membrane via the polyamic precursor route. aBPDA-P1 and 6FDA-P1 are prepared using the same method.

20 × 3 × 0.025 mm.

X-ray diffraction (XRD) studies were performed using a Bruker AXSD8 Discover diffractometer in transmission mode using a CuKα-radiation source. For every nanocomposite, four layers of the thin films were mounted on a support with the film surface orthogonal to the beam direction. The $Cu_3(BTC)_2$ MOF samples were quickly placed in between 2 scotch tapes and placed in the sample holder. The diffraction pattern was recorded at room temperature. Wide-angle XRD was performed using a distance of 6 cm between the sample and the detector and the exposure time was set to 5 min.

A Leica DM-LM optical microscope equipped with crossed polarizers and a hot stage was used to image ODPA-P1 polyamic acid and observe morphological changes during thermal imidization. Thermal imidization of the polyamic acid in NMP was performed by heating a drop of polyamic in between glass slides on a hot stage at 100 °C for 10 min with a cover slip to prevent escape of solvent and heating the obtained thin film to 320 °C at 10 °C/min.

A High-resolution JEOL scanning electron microscope (HR-SEM) operating at 5 kV was employed to study the fracture surfaces of the nanocomposites. The mixed matrix membranes were fractured by hand after immersing the membranes in liquid nitrogen for 15 min. After sputtering with gold, samples were placed in the SEM vacuum chamber and the electron beam was focused on the cross-sectional area of the fractured edge. A Thermo Electron Noran System Six energy-Dispersive X-ray spectrometer coupled to the SEM was used to identify the $Cu_3(BTC)_2$ MOFs in the MMMs. The accelerating voltage was increased to 15 kV and sample mapping was performed by recording for the duration of 6 min.

2.4. Gas separation measurements

Gas separation measurements were performed with a custom-built gas permeation set-up using a constant volume-variable pressure method, as described elsewhere [39]. The membranes were placed into a stainless steel cell and the permeate side was evacuated for 1 h. A gas feed comprising 50:50 mol.% CO_2 and CH_4 was used for all measurements. A feed pressure of 2 bars was applied at the top-side of the polyetherimide membranes. The permeate side was maintained under vacuum. The gas permeability values were calculated from the steady state pressure increase with

time in a well-calibrated (constant) volume at the permeate side. The permeability values are expressed in Barrer, where 1 Barrer = 10^{-10} cm^3 (STP) cm/(cm^2 s cmHg). All experiments were performed at a constant temperature of 35 °C. The composition of both the feed and the permeate were analyzed by a Varian 3900 GC gas chromatograph using an Alltech alumina F-1 60/80 packed bed column at 150 °C. The gas selectivity (α) was calculated by the following relationship:

$$\alpha_{i,j} = \frac{y_i / y_j}{x_i / x_j} \qquad \text{Equation (1)}$$

where y_i and y_j are the mole fractions of the components in the permeate, while x_i and x_j are their corresponding mole fractions in the feed. Eq. (1) is well known and used to calculate the mixed gas selectivity, as in the case of gas mixture, the presence of one component can severely influence the permeation behavior of the other components in the mixture. The permeability and selectivity values reported are the average of 2 membrane samples.

3. Results and discussions

3.1. Synthesis of polyamic acid

The viscosity of the polyamic acid intermediate increases within one hour of the onset of polymerization. Since the polyamic acid synthesis follows bimolecular reaction kinetics and the reverse reaction is unimolecular, the concentration of the monomers in NMP always needs to be the same for every polymerization (22 wt.% of NMP) in order to obtain reproducible molecular weights. The molecular weights of the polyamic acid intermediates for the three polymers measured after 24 h of stirring at 25 °C are listed in Table 1. The molecular weights (Mn) obtained are in the range of 60,000–70,000 g/mol for all three polymers.

Mixing the activated $Cu_3(BTC)_2$ with NMP solvent is exothermic due to filling of the empty pores of the MOF. This mixture was sonicated in a bath sonicator for 20 min. Previously published research from our group has shown that there is no degradation or change in structural features of $Cu_3(BTC)_2$ when subjected to such low intensity sonication [16]. Major structural changes in pore volume and size have only been previously observed when $Cu_3(BTC)_2$ in a solvent was subjected to > 1 h of intense sonication using a high intensity probe sonicator (750 Watts) [40]. The sole aim of low intensity sonication in this work is to achieve homogenous distribution of $Cu_3(BTC)_2$ in the polyamic acid precursor and therefore in the final polyetherimide films. After bath sonication, the $Cu_3(BTC)_2$-NMP solution was quickly added to the viscous polyamic acid solution while maintaining stirring. When we tried adding the $Cu_3(BTC)_2$ directly as a powder or without any prior sonication of the $Cu_3(BTC)_2$–NMP mixture to the polyamic acid solution, it resulted in large visible agglomerates of $Cu_3(BTC)_2$. Once agglomeration of $Cu_3(BTC)_2$ occurred, we were unable to re-disperse the $Cu_3(BTC)_2$ in the polyamic acid despite bath sonicating the solution for 1 h. Although decreasing the polyamic acid viscosity by dilution with NMP to ~10 wt.% solids enables good mixing of polyamic acid and $Cu_3(BTC)_2$ in solution, the $Cu_3(BTC)_2$ sediments when stirring is stopped or when films are cast. Sedimentation of $Cu_3(BTC)_2$ is not desirable since the $Cu_3(BTC)_2$ hydrolyzes when exposed to air. As $Cu_3(BTC)_2$ is extremely sensitive to air/moisture, sonication experiments and the polymerization reactions were maintained under inert gas atmosphere at all times.

The 1.5 ml of NMP utilized for dispersing $Cu_3(BTC)_2$ results in dilution of the polyamic acid intermediate from 22 wt.% to 18 wt.% of NMP. For sake of maintaining similar casting conditions, the casting of the neat polyamic acids was done only after dilution of the polyamic-acid intermediate solution to 18 wt.%.

Table 1
Molecular weights of polyamic-acid intermediates as determined by GPC.[a]

Polyetherimide	Mn (g/mol)	Mw (g/mol)	PDI
ODPA-P1	71,000	131,000	1.85
aBPDA-P1	60,000	122,000	1.70
6FDA-P1	72,000	109,000	1.85

[a] The fully imidized poly(etherimide)s are insoluble in NMP, hence only the molecular weights of the polyamic acid intermediates are reported.

3.2. Thermal imidization; polyamic acid intermediate to polyetherimide

Generally, the conversion of the polyamic acid intermediate to the polyimide is performed by thermal imidization of polyamic acid films in isothermal steps with a final imidization temperature of 300 °C for 1 h. However, the onset of $Cu_3(BTC)_2$ degradation occurs at roughly the same temperature (Fig. 1A). The color of the mixed matrix membrane also changes from dark blue to brownish–yellow when thermally imidized at 300 °C (Fig. 1B). When we analyzed ODPA-P1 with 10% $Cu_3(BTC)_2$ prepared by imidizing the films at 60 °C, 100 °C, 200 °C, 220 °C and 300 °C using Wide angle X-ray diffraction (WAXD), the characteristic peaks due to $Cu_3(BTC)_2$ disappear when imidized at 300 °C (Fig. 1S, Supporting Information).

The mechanism of thermal imidization of polyamic acid to polyimide is complex due to multiple processes occurring simultaneously. Furthermore, it is also dependent on several interdependent parameters such as molecular structure [41], residual solvent [42], imidization temperature and time of isothermal hold [43]. The extent of amic-acid conversion to imide via thermal imidization can be studied using FT-IR spectroscopy [43–46].

The FT-IR spectra obtained using the attenuated total reflection (ATR) method of neat membranes at different imidization temperatures are shown in Fig. 2S. In Fig. 2A, we have compared the spectra of neat membranes obtained after imidization at 220 °C and 300 °C. For sake of comparison, the FT-IR curves have been normalized using an internal standard *i.e.* the C–C aromatic stretch at 1490 cm^{-1}. The imide rings exhibit characteristic peaks centered at 1780 cm^{-1} (–C=O asymmetric stretching), ~1370 cm^{-1} (–CN symmetric stretching) and at 725 cm^{-1} (–C=O bending) [44,46]. Upon imidization at temperatures above 200 °C, the peaks due to –C=O in –COOH of polyamic acid at 1660 cm^{-1} (Fig. 2S) disappear. The perfect overlap of the FT-IR curves for films imidized at 220 °C and 300 °C (Fig. 2A) and the results obtained by quantification of the imide content (Fig. 2SD) indicates near complete imidization at 220 °C. The results for ODPA-P1 $Cu_3(BTC)_2$ mixed matrix membranes are shown in Fig. 2B. The results suggest no change in imide content due to $Cu_3(BTC)_2$ inclusion. Similar results were obtained for MMMs prepared using aBPDA-P1 and 6FDA-P1 matrices (spectra not shown). These results show that near-complete imidization can be achieved for these membranes at an imidization temperature of 220 °C (isothermal for 1 h) without any evidence of $Cu_3(BTC)_2$ decomposition.

3.3. Thermal stability: thermo-gravimetric analysis (TGA)

The thermal stability of the mixed matrix membranes was assessed using thermo-gravimetric analysis (TGA). The MMMs and the neat polymer matrices were heated from 25 °C to 600 °C under a nitrogen atmosphere at a heating rate of 10 °C/min. The results are presented in Fig. 3.

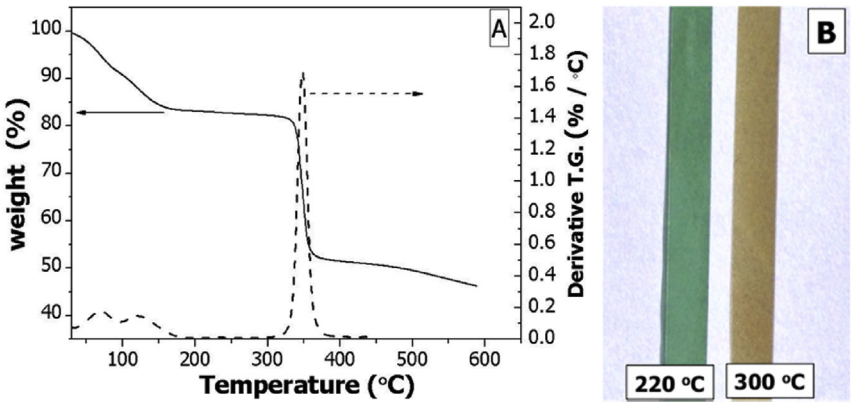

Fig. 1. A–The TGA analysis of crystalline $Cu_3(BTC)_2$ as a function of temperature was performed at 10 °C/min in N_2 atmosphere. The derivative of weight (%) as a function of temperature is shown on the right Y-axis. The onset of $Cu_3(BTC)_2$ degradation occurs at ~300 °C. B–Images of ODPA-P1 with 10% $Cu_3(BTC)_2$ when imidized by an isothermal hold (1 h in vacuum) at 220 °C and 300 °C. The color of the mixed matrix membrane changes from blue/green to brown, indicating decomposition of $Cu_3(BTC)_2$. (For interpretation of the references to colour in this figure legend, the reader is referred to the web version of this article.)

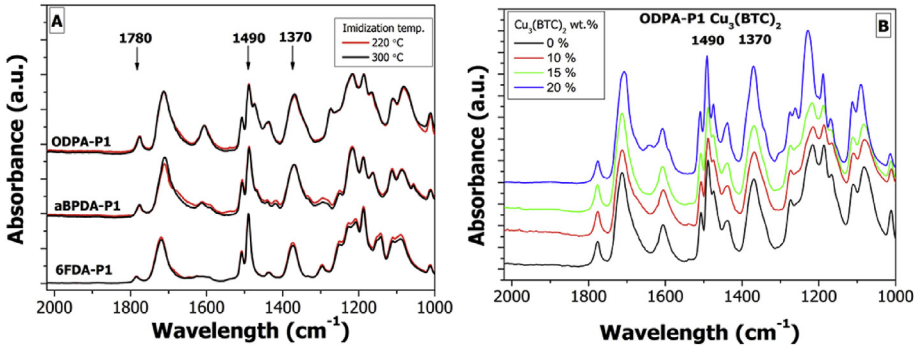

Fig. 2. Imidization analysis by FT-IR spectroscopy. A–FT-IR spectra for neat membranes imidized at 220 °C and 300 °C. The perfect overlap of the peaks at 1370 and 1490 cm^{-1} is indicative of near complete imidization. B–Comparison of ODPA-P1 $Cu_3(BTC)_2$ membranes obtained by imidizing at 220 °C. The area of the 1370 cm^{-1} peak is the same for all $Cu_3(BTC)_2$ loadings. All curves have been normalized using the peak at 1490 cm^{-1} (C–C aromatic stretch) as the internal reference.

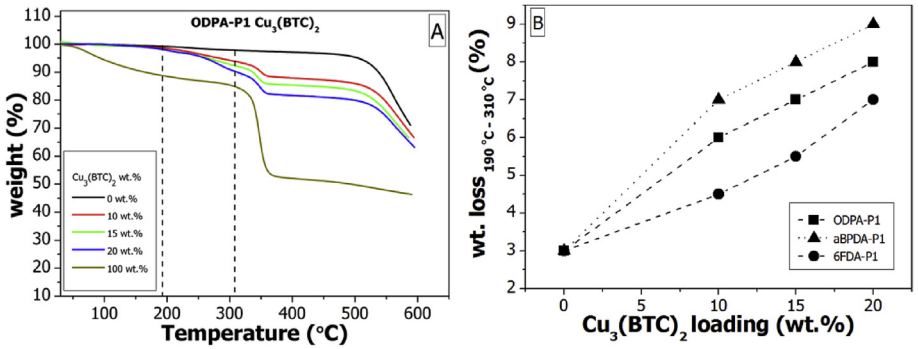

Fig. 3. TGA curves of ODPA-P1 with $Cu_3(BTC)_2$. A–Weight (%) as a function of temperature for all ODPA-P1 based mixed matrix membranes. $Cu_3(BTC)_2$ is included for sake of comparison with the mixed matrix membranes. The dotted lines indicate the region in which loss of NMP solvent occurs. The second major weight loss (onset ~320 °C) in the membranes is due to degradation of $Cu_3(BTC)_2$ in ODPA-P1. The weight loss corresponds to the amount of $Cu_3(BTC)_2$ incorporated in ODPA-P1. B–Weight loss (%) of NMP for all mixed matrix membranes as a function of $Cu_3(BTC)_2$ loading in the temperature region 190 °C–315 °C.

The TGA and derivative thermo-gravimetric (DTG) (%/°C) curves for ODPA-P1 $Cu_3(BTC)_2$ are shown in Fig. 3A and Fig. 3S. Similar curves for 6FDA-P1 and aBPDA-P1 $Cu_3(BTC)_2$ are shown in Fig. 4S. From Fig. 3A, it is clear that ODPA-P1 polyetherimide degrades at ~530 °C due to thermal decomposition. In the MMMs, the onset of degradation of the polymer backbone also occurs at 530 °C. But all the MMMs also exhibit significant weight loss in the temperature region 190 °C–310 °C followed by another larger weight loss in the region of ~320 °C. The weight loss occurring at 320 °C is due to degradation of the organic linkers in $Cu_3(BTC)_2$. This weight loss also coincides with the degradation onset (Fig. 3A) of neat $Cu_3(BTC)_2$. Using direct probe mass spectroscopy, we heated small quantities of our MMMs to 250 °C at 10 °C/min inside the mass spectrometer. The only molecule detected by the mass spectrometer was the solvent NMP. The presence of residual solvent in these films is not surprising. Polyimides are known to retain solvent

when imidized at temperatures well below 300 °C, which is the reason that the thermal imidization procedure is generally performed up to 300 °C [47]. Additionally, the non-imidized polyamic functionalities (<~2%) can undergo further imidization by eliminating water during heating up to 300 °C in the TGA. Since we have limited the final imidization temperature to only 220 °C, we can expect the membranes to retain a higher amount of NMP —the neat ODPA-P1 contains ~3% NMP while ODPA-P1 imidized at 300 °C does not show weight loss in this temperature region (Fig. 3A). $Cu_3(BTC)_2$ is also known to be strongly solvated by solvents such as NMP and needs to be heated to temperatures up to 220 °C to remove all solvent prior to use [48]. But when embedded in polymeric matrices, the complete removal of solvents such as NMP can be anticipated to be extremely difficult.

By plotting the DTG (%/°C) curves for the mixed matrix membranes (Figs. 3S and 4S), it is clear that the NMP solvent loss in the 190 °C–310 °C region increases as the $Cu_3(BTC)_2$ MOF loading is increased. By quantifying the weight loss in the 190–310 °C region (Fig. 3B), we find a linear relationship for all matrices as a function of $Cu_3(BTC)_2$ loading. At 20 wt.% $Cu_3(BTC)_2$, all mixed matrix membranes contain ~7–9% of NMP. The peak temperature of the solvent loss from the DTG curves increases by ~40 °C (Fig. 4SE) when 10% $Cu_3(BTC)_2$ is added and then plateaus for all three matrices. These results taken together imply that most of the NMP in the mixed matrix membranes is concentrated in or close to the $Cu_3(BTC)_2$ particles, *i.e.* the interphase region will be strongly affected by residual solvent.

The results obtained prove that the addition of $Cu_3(BTC)_2$ to poly(etherimide)s results in retention of ~8 wt.% solvent at 20 wt.% $Cu_3(BTC)_2$. The presence of residual solvent will have repercussions on the morphology of the polymer chains at the interface and strongly influence the overall gas transport behavior of the MMMs. The effects of residual solvent at the $Cu_3(BTC)_2$–polymer interface on polymer packing or gas transport has not been addressed in previous literature [25,49].

3.4. Membrane morphology; crystallinity

The inclusion of $Cu_3(BTC)_2$ is expected to induce changes in the molecular packing of the polymer chains. To study the morphological changes in the polymer matrix, we performed WAXD studies on the MMMs and bulk $Cu_3(BTC)_2$ powder (Fig. 4).

In Fig. 4A, we have shown the WAXD reflections of the as-received $Cu_3(BTC)_2$. A second batch of $Cu_3(BTC)_2$ was sonicated in NMP followed by filtration under Argon and subsequently heated up to 220 °C in an Argon purged vacuum oven to mimic the thermal imidization process. The WAXD reflections of both sets of $Cu_3(BTC)_2$ powders match the results reported in literature. This implies that the crystal structure is maintained even when $Cu_3(BTC)_2$ is sonicated in NMP and heated up to 220 °C in a vacuum oven. A major difference between the two curves is in the relative intensities of the peaks *e.g.* compare peaks centered at 2θ of 6.7° and 11.5°. Presumably, this is due to presence of NMP solvent in the pores of $Cu_3(BTC)_2$ [48,50].

In Fig. 4B, the WAXD curves as a function of 2θ are shown for ODPA-P1 $Cu_3(BTC)_2$ membranes. The reflections corresponding to $Cu_3(BTC)_2$ are visible in the MMMs indicating that the crystal structure of $Cu_3(BTC)_2$ has remained intact during the synthetic procedure. But significant differences in intensities of the 2θ peaks centered at 6.7, 9.5, 11.5 and 13.5° are observed when compared to neat $Cu_3(BTC)_2$. Presumably, the pore filling of $Cu_3(BTC)_2$ with NMP solvent and the interference from the underlying amorphous polyetherimide diffraction pattern are responsible for such changes in relative peak intensity of $Cu_3(BTC)_2$. Similar changes in peak intensities associated to $Cu_3(BTC)_2$ are also observed in the WAXD results for aBPDA-P1 $Cu_3(BTC)_2$ (Fig. 4C) and 6FDA-P1 $Cu_3(BTC)_2$ (Fig. 4D).

However, in ODPA-P1 $Cu_3(BTC)_2$ the peaks centered at 2θ values of 3.5, 17.3 18.9 and 25.8° are unusually large and broad compared to the $Cu_3(BTC)_2$ as-received powder or when compared to 6FDA-P1 or aBPDA-P1 based membranes. ODPA-P1 polyetherimide has been shown to form ordered, crystal domains when films are cast from dilute polyamic acids (10 wt.% concentration). [33]. This solvent induced crystallinity is confirmed by the presence of a cold crystallization peak at 260 °C when an ODPA-P1 film is prepared from a 10 wt.% polyamic acid solution followed by thermal imidization up to 220 °C (Fig. 5SA). Cold crystallization does not occur in neat ODPA-P1 prepared from 15to 20 wt.% polyamic acid, hence the amorphous polymer. We also found that the crystallization temperature decreased when the amount of residual solvent was increased. When NMP (>5 wt.%) was trapped inside the film, we were able to crystallize the polymer at ~200 °C during imidization (Fig. 5SB). A WAXD analysis (Fig. 6S) of a semi-crystalline ODPA-P1 film confirms that the peaks at 3.5, 17.3, 18.9 and 25.8° are associated with crystalline domains in ODPA-P1. These reflections are also present in the ODPA-P1 $Cu_3(BTC)_2$ membranes. These results prove that the retention of NMP by $Cu_3(BTC)_2$ in the ODPA-P1 membranes aids in crystallization of the polymer chains.

In summary, the crystalline structure of $Cu_3(BTC)_2$ is maintained when incorporated within the three polyetherimide matrices. The inclusion of $Cu_3(BTC)_2$ induces crystallization in the ODPA-P1 matrix whereas 6FDA-P1 and aBPDA-P1 remain fully amorphous.

3.5. Membrane morphology; the glass transition (Tg)

The analysis of the Tg event can provide information on the organization of the amorphous chains in mixed matrix membranes. In the field of traditional (macro– and nano–) composites, a tremendous amount of research has been published on the Tg event of the polymer matrix in the presence of organic and inorganic fillers [51–53].

In this research article, we report on the changes in Tg due to $Cu_3(BTC)_2$ addition using results obtained from first heat differential scanning calorimetry (DSC) measurements. We have only considered the first heat since the films have been used for gas separation measurements as produced, *i.e.* without any annealing of the MMMs above Tg. A number of reports on MMMs, containing MOF fillers, have reported the Tg during the second or third heating cycle, this is erroneous since heating/cooling cycles affect chain packing by removal of solvent, degradation of the MOF filler and by eliminating the thermal history.

The Tg results as obtained by DSC are tabulated in Table 2 and the DSC curves are presented in Figs. 5 and 6. All DSC experiments were performed at 20 °C/min. under an inert N_2 atmosphere. The sample size used for DSC measurement was ~8 mg. All curves have been normalized to the polymer weight in the sample *i.e.* the weight of $Cu_3(BTC)_2$ in the membranes was subtracted from the DSC samples since the MOFs do not participate in the Tg event.

In Fig. 5A, the Tg curves for ODPA-P1 imidized at 220 °C and 300 °C are shown. The Tg event for ODPA-P1 when imidized by an isothermal hold at 300 °C for 1 h occurs at 244 °C, *i.e.* 16 °C higher than when imidized at 220 °C (Fig. 5A). Applying a high temperature (300 °C) thermal imidization step, above the Tg of the polyimide, eliminates residual NMP solvent and the additional imidization results in an increase in chain packing density [54]. Consequently, these physical processes result in stronger interchain interactions rendering the polyetherimide chains more conformational rigid. The associated reduction in free volume results in higher Tg values. Similar results were obtained for aBPDA-P1 and 6FDA-P1 and are shown in Fig. 7S. Based on these results, we

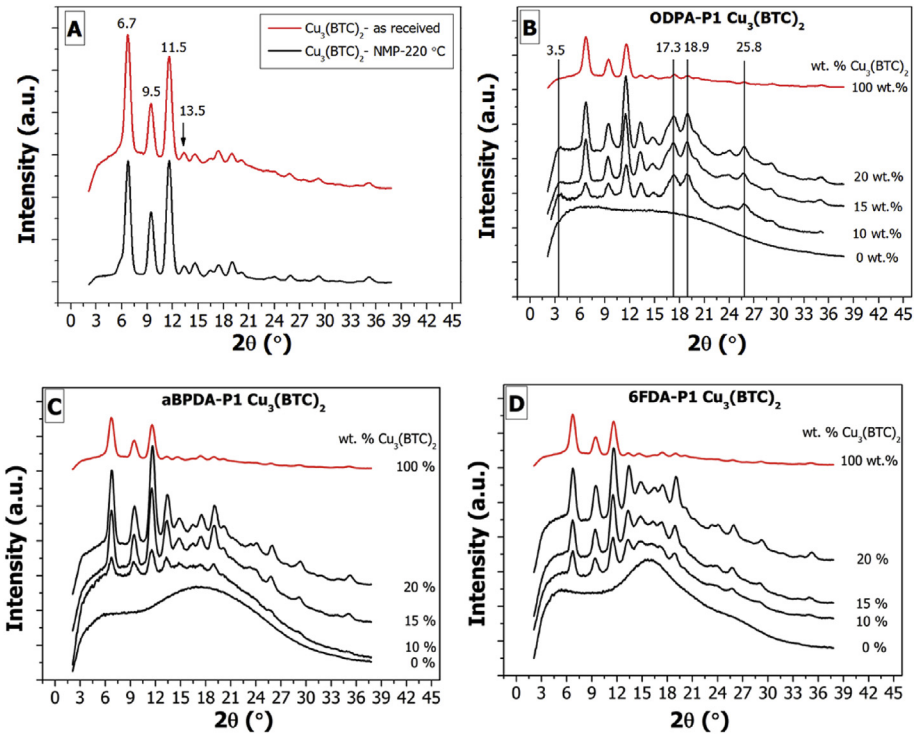

Fig. 4. Wide angle X-ray diffraction (WAXD) studies on $Cu_3(BTC)_2$ and MMMs. A—WAXD of powdered $Cu_3(BTC)_2$ as received. A second sample was prepared by sonicating $Cu_3(BTC)_2$ in NMP solvent for 20 min under a N_2 atmosphere, filtered and then heated in the oven to mimic the imidization procedure. WAXD curves for B—ODPA-P1 $Cu_3(BTC)_2$, C—aBPDA-P1 $Cu_3(BTC)_2$ and D-for 6FDA-P1 $Cu_3(BTC)_2$ mixed matrix membranes as a function of 2θ. All curves for the MMMs have been normalized to sample thickness and arranged vertically for sake of clarity. The intensity of $Cu_3(BTC)_2$ has been reduced by a factor of 100 for easy comparison.

Table 2
Thermal and thermo-mechanical properties of the mixed matrix membranes.

Matrix	$Cu_3(BTC)_2$ content (wt. %)	Tg by DSC (°C)[a]	ΔCp (J/(°C g))	E′ at 30 °C (GPa)[b]	Tg (°C) DMTA[c]	Morphology[d]
ODPA-P1	0	230	0.22	3.7	237	Am.
	10	227	0.18	4.2	237	SC.
	15	228	0.04	5.3	242	SC.
	20	228	0.02	7.3	243	SC.
aBDPA-P1	0	242	0.10	2.7	286	Am.
	10	249	0.14	2.8	284	Am.
	15	250	0.07	2.9	278	Am.
	20	250	0.02	2.3	284	Am.
6FDA-P1	0	253	0.18	4.0	280	Am.
	10	259	0.09	4.0	274	Am.
	15	253	0.13	4.2	272	Am.
	20	235	0.12	4.0	264	Am.

[a] Tg was determined at the inflection point. DSC measurements were performed at a heating rate of 20 °C/min. under a N_2 atmosphere.
[b] Storage moduli were obtained at 30 °C and at frequency of 1 Hz
[c] Tg is reported at the maximum of the loss modulus (E″).
[d] The morphology was determined from wide angle X-ray diffraction measurements; Am = amorphous, SC = semi-crystalline.

want to emphasize the importance of the synthetic procedures, such as the final thermal imidization temperature used to produce polyimide– and polyetherimide–based MMMs.

The addition of $Cu_3(BTC)_2$ to ODPA-P1 results in crystallization of the polymer chains (Fig. 4B). The crystalline domains of ODPA-P1 do not participate in the Tg event. This is reflected in the decreasing ΔCp values at the Tg, *i.e.* from 0.22 for neat to 0.02 J/(°C.g) at 20 wt.% $Cu_3(BTC)_2$ (Table 2, Fig. 5B). The Tg event occurs at ~228 °C for all ODPA-P1 based membranes. Since we have not been able to calculate the % crystallinity induced due to $Cu_3(BTC)_2$ inclusion in ODPA-P1, the DSC results cannot be used to ascertain if a significant amount of amorphous polymer also exists as rigid amorphous polymer.

In poly(etherimide)s containing the asymmetric, highly kinked, aBPDA dianhydride, the cooperative segmental motion of the repeat unit is highly hindered [34]. The Tg for neat aBPDA-P1, imidized at 220 °C, is at 240 °C and also exhibits a relaxation enthalpy (Fig. 6A). With inclusion of $Cu_3(BTC)_2$, onset of the Tg event remains nearly unchanged compared to neat aBPDA-P1 (~235 °C) although the Tg event occurs over a wider temperature range. The broadening of the Tg and the use of the inflection point for denotation of a single Tg temperature results in a higher Tg (~250 °C) being marked for aBPDA-P1 $Cu_3(BTC)_2$ membranes. The broadening of the Tg event indicates the presence of several Tg events that cannot be de-convoluted. The reduction in ΔCp values from 0.10 for neat to 0.02 J/(°C.g) at 20 wt.% $Cu_3(BTC)_2$ is a reflection of this broadening. These results are consistent with the presence of NMP solvent within amorphous membranes. These results seem to suggest that the inclusion of $Cu_3(BTC)_2$ does not drastically affect the arrangement of the amorphous aBPDA-P1 polymer chains.

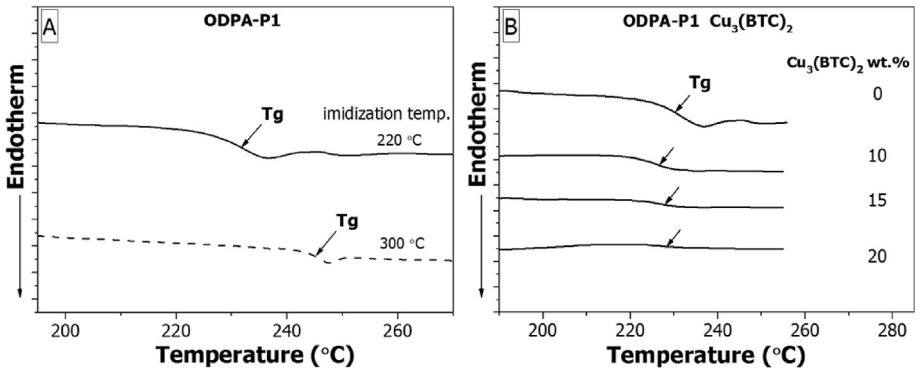

Fig. 5. DSC curves at the Tg for ODPA-P1 with $Cu_3(BTC)_2$. All curves have been normalized to sample weight and arranged for sake of clarity. A–Tg curves for ODPA-P1 obtained by imidizing at 220 °C and 300 °C. B–DSC curves at the Tg as a function of temperature for the ODPA-P1 $Cu_3(BTC)_2$ membranes. The arrows indicate the Tg event.

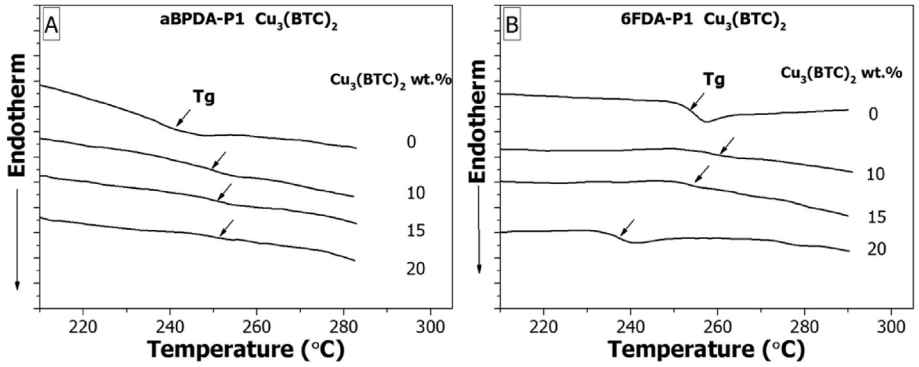

Fig. 6. DSC curves at the Tg as a function of temperature for A-aBPDA-P1 $Cu_3(BTC)_2$ and B–6FDA-P1 $Cu_3(BTC)_2$ membranes. All curves have been normalized to polymer sample weight and have arranged vertically for sake of clarity. The arrows indicate the Tg event.

The 6FDA-P1 polyetherimide is a rigid polymer with weak interchain interactions due to the presence of two bulky $-CF_3$ groups. The 6FDA-P1 polyetherimide, when prepared by imidizing at a final temperature of 220 °C, has a Tg of 253 °C. At 10 wt.% $Cu_3(BTC)_2$ content, the Tg increases to 259 °C and broadens, indicating the presence of overlapping multiple Tg events. However, increasing the $Cu_3(BTC)_2$ content to 15 and 20 wt.% alters the relaxation dynamics dramatically, causing the Tg to occur at lower temperatures *i.e.* at 253 °C and 235 °C respectively (Fig. 6B). Compared to ODPA-P1 and aBPDA-P1 poly(etherimide)s, the 6FDA-P1 is capable of interacting more strongly with the polar NMP solvent and $Cu_3(BTC)_2$ due to the presence of local dipoles ($-CF_3$ groups) [55,38], Also, changes in rate of thermal imidization due to retention of NMP solvent by $Cu_3(BTC)_2$ (Fig. 3B) will adversely affect chain packing. [42]. The decrease in Tg of ~18 °C at 20 wt.% $Cu_3(BTC)_2$ suggests larger free volume than in the neat.

3.6. Dynamic mechanical thermal analysis (DMTA)

The thermo-mechanical behavior of the mixed matrix membranes *i.e.* the storage modulus (E′) as function of temperature was studied using DMTA. All membranes were tested at a constant heating rate of 2 °C/min and at a frequency of 1 Hz. The results obtained are shown in Fig. 7 and listed in Table 2.

The ODPA-P1 polymer exhibits typical amorphous polymer characteristics when analyzed by DMTA. The storage modulus (E′) at 30 °C is ~3.7 GPa and the storage modulus drops immediately after the Tg (Fig. 7A). The incorporation of 20 wt.% $Cu_3(BTC)_2$ increases the E′ from 3.7 GPa to 7.3 GPa at 30 °C. This increase in storage modulus is due to the presence of crystalline domains induced by the addition of $Cu_3(BTC)_2$. Above Tg, ODPA-P1 containing 10 wt.% $Cu_3(BTC)_2$ exhibits a rubber plateau typically observed in semi-crystalline polymeric materials. The unusually low drop in storage modulus after the Tg in ODPA-P1 membranes containing 15 and 20 wt.% $Cu_3(BTC)_2$ is indicative of the presence of rigidified amorphous polymer. The drop in E′ above Tg is followed by a rubber plateau due to molecular entanglements with the crystalline blocks. These results are consistent with the results from WAXD and Tg studies using DSC and confirms the presence of a rigid polymer network in ODPA-P1 $Cu_3(BTC)_2$.

The aBPDA-P1 and 6FDA-P1 based MMMs are amorphous membranes with room temperature storage moduli of 2.7 and 4.0 GPa, respectively. For both series of MMMs, a rubber plateau above the Tg is observed only at 15 and 20 wt.% $Cu_3(BTC)_2$. Presumably, addition of 15 or 20 wt.% $Cu_3(BTC)_2$ causes confinement of polymer chains resulting in increased amount of molecular entanglements.

If the E′ at 30 °C for all MMMs is plotted as a function of wt.% $Cu_3(BTC)_2$ (Fig. 7D), an approximately exponential increase in E′ is only observed for the OPDA-P1 based membranes. The storage modulus values remain near constant for aBPDA-P1 and 6FDA-P1 $Cu_3(BTC)_2$. In fact, in aBPDA-P1 20% $Cu_3(BTC)_2$ the storage modulus value at 30 °C is lower than the neat polymer by 0.4 GPa suggesting the presence of voids at the MOF-polymer interface. The lack of an increase in E′ for aBPDA-P1 and 6FDA-P1 based MMMs can be attributed to the presence of amorphous chains along with residual NMP at the $Cu_3(BTC)_2$-polymer interface. It is a reflection of the conformational rigidity of aBPDA-P1 and 6FDA-P1 preventing the polymer chains from forming ordered domains along the $Cu_3(BTC)_2$ surface.

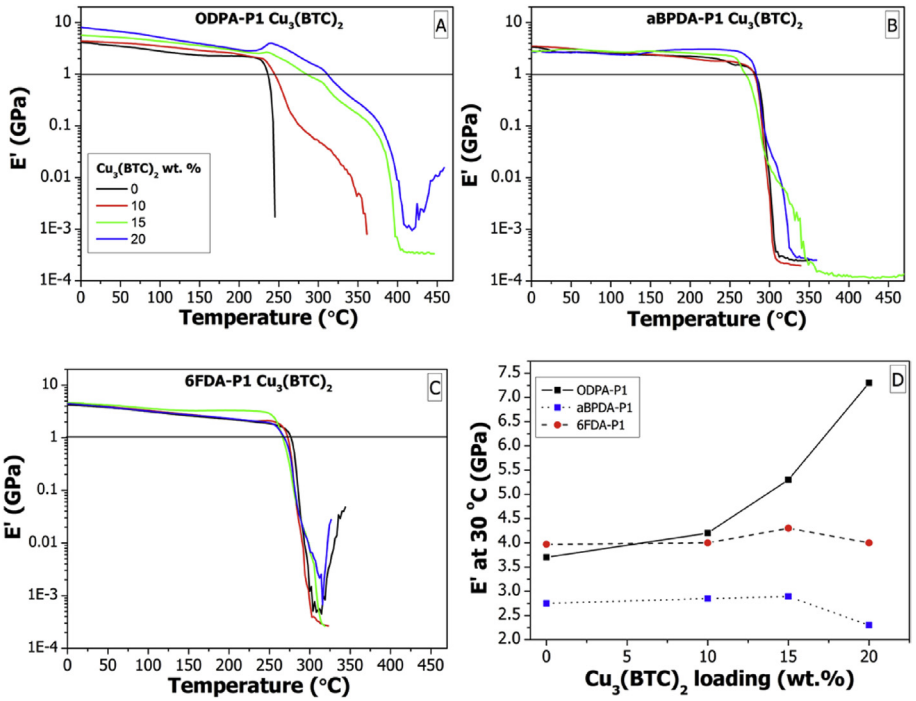

Fig. 7. Storage modulus (E′) as a function of temperature for the neat polymers and their MMMs. A—ODPA-P1 $Cu_3(BTC)_2$ B—aBPDA-P1 $Cu_3(BTC)_2$ and C—6FDA-P1 $Cu_3(BTC)_2$. The overshoot of E′ at the Tg in ODPA-P1 $Cu_3(BTC)_2$ (Fig. 7A) is due to stress relief. The legend for all three figures is provided in Fig. 7A. The DMTA analyses for all membranes were performed at a frequency of 1 Hz and at 2 °C/min under a N_2 atmosphere. D—Storage moduli at 30 °C and 1 Hz as a function of $Cu_3(BTC)_2$ loading in the membranes.

3.7. Gas separation measurements

The results for the gas separation measurements of the neat membranes and the mixed matrix membranes containing 20 wt.% $Cu_3(BTC)_2$ are summarized in Table 3. The presented data is the averaged result from two membranes. The difference in permeability values obtained for the two membranes was in the range of ~5%.

The permeability and selectivity values for CO_2 in the ODPA-P1 neat membrane are typical of rigid polymeric membranes [32]. The obtained permeability values of 1.18 and 0.18 Barrers for CO_2 and CH_4, respectively, in neat ODPA-P1 match the values reported by Simons et al. [32]. The presence of a crystalline, rigidified polymer at 20 wt.% $Cu_3(BTC)_2$ results in reduction of the CO_2 permeability from 1.18 to 0.97, along with an increase in CO_2/CH_4 selectivity from 41.5 to 52.0. We believe that separation of CO_2 and CH_4 occurs via a sieving mechanism due to the presence of $Cu_3(BTC)_2$ and rigid polymer domains (both crystalline and rigid amorphous polymer).

The decrease in permeability observed at 20 wt.% $Cu_3(BTC)_2$ can be attributed to the rigidification of polymer chains due to presence of crystalline domains and the absence of non-selective voids [18]. As observed from SEM images shown in Fig. 8, $Cu_3(BTC)_2$ is completely coated with polymer and the $Cu_3(BTC)_2$ – ODPA-P1 interface appears to be devoid of any non-selective voids.

However, we speculate that the increase in selectivity value from 41.5 to 52.0 is due to a combined effect of rigidified polymer (crystalline and rigid amorphous polymer) and the presence of $Cu_3(BTC)_2$. The rigidified polymer in ODPA-P1 can contribute to an increase in the diffusion selectivity of the composite. The unsaturated metal coordination sites in $Cu_3(BTC)_2$ may aid in increasing selectivity by interacting more strongly with the partially charged (quadruple moment) CO_2 molecules than with CH_4. This is also evident in the higher heat of adsorption values for CO_2 (25 kJ/mol) compared to CH_4 (15 kJ/mol) [56]. Additionally, $Cu_3(BTC)_2$ has smaller triangular windows (0.35 nm) connecting the main channels that are known to aid in the sieving of gas molecules.

The inclusion of 20 wt.% $Cu_3(BTC)_2$ in aBPDA-P1 results in an increase of 68% in permeability for both CO_2 and CH_4. But the increase in permeability is not accompanied by a corresponding increase in selectivity that remains constant at ~42. The 68% increase in permeability for CO_2 and CH_4 is indicative of a similar diffusion pathway for both of these gases. Although the small increase in permeability may be attributed to the incorporation of $Cu_3(BTC)_2$, the lack of selectivity increase is most probably due to the presence of non-selective voids at the $Cu_3(BTC)_2$-polymer interface. When cross-sections of aBPDA-P1 20 wt.% $Cu_3(BTC)_2$ membranes were

Table 3
Gas permeation and separation performance of MMMs using 50:50 CO_2/CH_4 feed.[a]

Matrix	$Cu_3(BTC)_2$ content (wt. %)	Morphology	CO_2 permeability (barrer)	CH_4 permeability (barrer)	Selectivity α (–)
ODPA-P1	0	Am.	1.18	0.03	41.5
	20	SC.	0.97	0.02	52.0
aBPDA-P1	0	Am.	2.64	0.06	42.0
	20	Am.	4.45	0.10	43.0
6FDA-P1	0	Am.	3.25	0.13	25.2
	20	Am.	4.92	0.14	33.5

[a] All measurements were performed at 2 bars and at 35 °C and all measurements were repeated twice using two different samples.

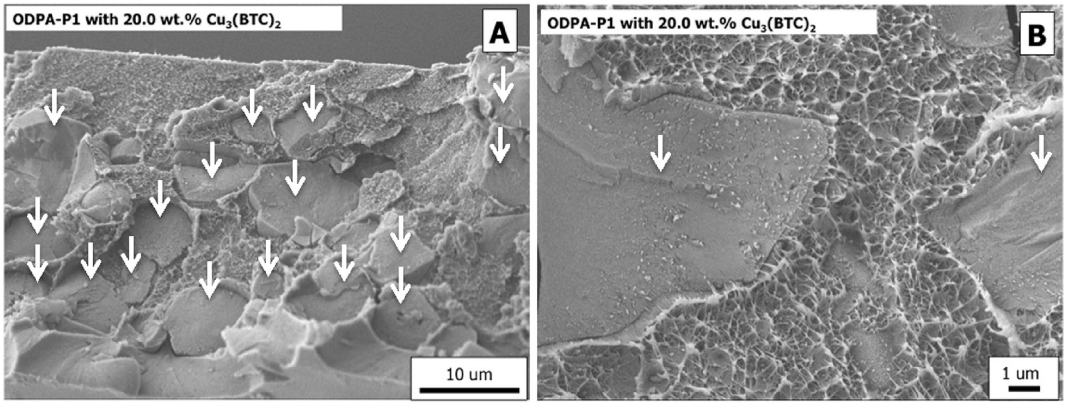

Fig. 8. Scanning electron microscopy (SEM) images of cross-sections of ODPA-P1 containing 20 wt.% $Cu_3(BTC)_2$. The films were fractured using a cryo-fracture technique. Two separate areas of the membrane are shown in Fig. 8A and B at two different magnifications. The white arrows point to $Cu_3(BTC)_2$ particles, which were identified by energy-dispersive X-ray spectroscopy (EDX) (Fig. 8S). The ODPA-P1 appears to completely coat the $Cu_3(BTC)_2$ particles and no voids are visible at the interface. The image of a cross-section of neat ODPA-P1 is shown in Fig. 9S.

analyzed by SEM (Fig. 10SA), voids were indeed visible at the $Cu_3(BTC)_2$-polymer interface, a typical sieve-in-a-cage morphology [14]. The formation of voids at the interface between $Cu_3(BTC)_2$ and aBPDA can be rationalized by considering the lack of conformational flexibility of the highly kinked aBPDA-P1 polymer backbone. It must be noted that it is not clear how many of these voids are the result of the cryo-fracture process utilized for preparing SEM samples and/or due to shrinkage of polymer arising from removal of NMP solvent during cryo-fracture.

6FDA-P1 polyetherimide exhibits higher permeability compared to the two other poly(etherimide)s that can be attributed to the presence of higher free volume due to two bulky $-CF_3$ groups. On addition of 20 wt.% $Cu_3(BTC)_2$ in 6FDA-P1, the permeability of CO_2 increases from 3.25 to 4.92 Barrers whereas the CH_4 permeability remains nearly constant. When compared to the neat polyetherimide, a substantial 32% increase in selectivity is obtained. It is not often that increases in both permeability and selectivity are obtained from inclusion of $Cu_3(BTC)_2$ in a polymeric membrane. The increase in selectivity implies the absence of voids at the 6FDA-P1–$Cu_3(BTC)_2$ interface. This can be confirmed by viewing the SEM image of the membrane cross-section (Fig. 10SB). From DSC investigation of the Tg event (Fig. 6B), we know that 6FDA-P1 containing 20 wt.% $Cu_3(BTC)_2$ has a larger free volume compared to the neat membrane. However, from the work of Coleman et al., it is clear that even the distribution of free volume affects gas permeability and selectivity [57]. The presence of NMP and $-C(CF_3)$ groups add to the complexity due to changes induced in the sorption and diffusion behavior [55]. Perhaps, the increase in free volume enables larger volume of gas molecules to access the pores of $Cu_3(BTC)_2$ thereby contributing to selectivity increasing. While these results are encouraging, a lot more work is required to understand and quantify the actual contribution of $Cu_3(BTC)_2$ towards gas transport in 6FDA-P1.

4. Conclusions

Mixed matrix membranes containing homogenously distributed, crystalline $Cu_3(BTC)_2$ MOFs in three different poly(etherimide)s based on ODPA-P1, aBPDA-P1 and 6FDA-P1 were synthesized using an *in-situ* polymerization technique and subsequent thermal imidization up to 220 °C. A key observation about the mixed matrix membranes was the retention of nearly 8 wt.% NMP even after solvent evaporation and thermal imidization at 220 °C. Consequently, the linear and flexible ODPA-P1, due to its propensity to crystallize in the presence of 'excess' solvent formed crystalline domains. This is also evidenced in the storage modulus increase with $Cu_3(BTC)_2$ loading, reduction in ΔCp at Tg and lower gas permeability compared to the neat membrane. In contrast, the highly kinked aBPDA-P1 is unable to undergo conformational alterations to 'adjust' to the presence of $Cu_3(BTC)_2$ resulting in non-selective voids, hence a ~68% increase in permeability of both CO_2 and CH_4 is observed without any corresponding increase in selectivity. With 20 wt.% $Cu_3(BTC)_2$ inclusion in 6FDA-P1, the amorphous polymer chains adopt a conformation resulting in larger free volume (and presumably with a different free volume distribution) compared to the neat membrane. This result is counterintuitive given the inherent conformational rigidity of 6FDA-P1. The net effect on gas transport observed is an increase in the permeability of CO_2 by ~68% along with a 33% increase in selectivity.

The point we wish to make here is that understanding the underlying polymer morphological changes due to MOF inclusion allows for rationalization of gas permeation and selectivity results. The results reported herein show that selecting the appropriate polymer matrix is crucial for improved gas transport. The results for 6FDA-P1 prove that both permeability and selectivity of MMMs based on such rigid, aromatic polymers can significantly increase by $Cu_3(BTC)_2$ incorporation.

Funding sources

Kitty Nijmeijer was awarded an Aspasia grant from Netherlands Organization for Scientific Research (NWO) to conduct this research.

Appendix A. Supplementary data

Supplementary data related to this article can be found at http://dx.doi.org/10.1016/j.polymer.2015.11.002.

References

[1] H. Yehia, T.J. Pisklak, J.P. Ferraris, K.J. Balkus Jr., I.H. Musselman, Polym. Prepr. 45 (2004) 35–36.
[2] J. Gascon, U. Aktay, M.D. Hernandez-Alonso, G.P.M. van Klink, F. Kapteijn, J. Catalysis 261 (2009) 75–87.
[3] Z.Q. Wang, S.M. Cohen, Chem. Soc. Rev. 38 (2009) 1315–1329.
[4] H.K. Chae, D.Y. Siberio-Perez, J. Kim, Y. Go, M. Eddaoudi, A.J. Matzger, M. Keeffe, O.M. Yaghi, Nature 427 (2004) 523–527.
[5] M. Eddaoudi, J. Kim, N. Rosi, D. Vodak, J. Wachter, M. O'Keeffe, O.M. Yaghi, Science 295 (2002) 469–472.
[6] E.V. Perez, K.J. Balkus Jr., J.P. Ferraris, I.H. Musselman, J. Memb. Sci. 328 (2009)

165–173.
[7] T. Loiseau, C. Serre, C. Huguenard, G. Fink, F. Taulelle, M. Henry, T. Bataille, G. Ferey, Chem Eur J. 10 (2004) 1373–1382.
[8] B. Zornoza, C. Tellez, J. Coronas, J. Gascon, F. Kapteijn, Micro. and Meso. Mater. 166 (2013) 67–68.
[9] S. Keskin, J. Liu, J.K. Johnson, D.S. Scholl, Micro. Meso Mater. 125 (2009) 101–106.
[10] S. Couck, J.F.M. Denayer, G.V. Baron, T. Remy, J. Gascon, F. Kapteijn, J. Am. Chem. Soc. 131 (2009) 6326–6327.
[11] J. Yang, A. Grzech, F.M. Mulder, T.J. Dingemans, Chem Commun. 47 (2011) 5244–5246.
[12] C.M. Zimmerman, A. Singh, W.J. Koros, J. Memb. Sci. 137 (1997) 145–154.
[13] G. Golemme, J.C. Jansen, M. Daniela, A. Bruno, M. Raffaella, M.G. Giovanna, J. Choi, M. Tsapatsis, in: Y. Yampolskii, B. Freeman (Eds.), Membrane Gas Separation, first ed., John Wiley & Sons, United Kingdom, 2010, p. 111.
[14] T.T. Moore, W.J. Koros, J. Mol. Struct. 739 (2005) 87–98.
[15] S. Husain, W.J. Koros, J. Memb. Sci. 288 (2007) 195–207.
[16] J. Ploegmakers, S. Japip, K. Nijmeijer, J. Memb Sci. 428 (2013) 445–453.
[17] J. Ploegmakers, S. Japip, K. Nijmeijer, J. Memb Sci. 428 (2013) 331–340.
[18] S. Shahid, K. Nijmeijer, J. Memb Sci. 470 (2014) 166–177.
[19] S. Shahid, K. Nijmeijer, J Memb. Sci. 459 (2014) 33–44.
[20] X.Y. Chen, H. Vinh-Thang, D. Rodrigue, S. Kaliaguine, Ind. Eng Chem Res. 51 (2012) 6895–6906.
[21] O.G. Nik, X.Y. Chen, S. Kaliaguine, J .Memb Sci. 413–414 (2012) 48–61.
[22] A. Car, C. Stropnik, K.-V. Pienemann, Desalination 200 (2006) 424–426.
[23] R. Adams, C. Carson, J. Ward, R. Tannenbaum, W.J. Koros, Micro. Meso Mater. 131 (2010) 13–20.
[24] Y. Zhang, I.H. Musselman, J.P. Ferraris, K.J. Balkus Jr., J. Membr. Sci. 313 (2008) 170–181.
[25] S. Basu, A. Cano-Odena, I.F.J. Vankelecom, J. Memb. Sci. 362 (2010) 478–487.
[26] T. Rodenhas, M. van Dalen, E. Garcia-Perez, P. Serra-Crespo, B. Zornoza, F. Kapteijn, J. Gascon, Adv. Func Mat. 24 (2014) 249–256.
[27] T.-H. Bae, J.S. Lee, W. Qiu, W.J. Koros, C.W. Jones, S. Nair, Angew Chem Int Ed. 49 (2010) 9863–9866.
[28] O. Ghaffari, X.Y. Chen, S. Kaliaguine, J. Memb Sci. 413–414 (2012) 48–61.
[29] S. Keskin, J. Liu, J.K. Johnson, D.S. Scholl, Micro. Meso Mater 125 (2009) 101–106.
[30] C. Zhou, L. Cao, S. Wei, Q. Zhang, L. Chen, Comp. Theoret Chem. 976 (2011) 153–160.
[31] T.J. Dingemans, E. Mendes, J.J. Hinkley, E.S. Weiser, T.L. St Clair, Macromolecules 41 (2008) 2474–2483.
[32] K. Simons, K. Nijmeijer, J.G. Sala, H. van der Werf, N.E. Benes, T.J. Dingemans, M. Wessling, Polymer 51 (2010) 3907–3917.
[33] S. Srinivas, M. Graham, M.H. Brink, S. Gardner, R.M. Davis, J.E. McGrath, G.L. Wilkes, Poly Engg Sci. 36 (1996) 1928–1940.
[34] M. Hasegawa, N. Sensui, Y. Shindo, R. Yokota, Macromolecules 32 (1999) 387–396.
[35] T.-H. Kim, W.J. Koros, G.R. Husk, K.C. O'Brien, J. Memb. Sci. 37 (1988) 45–62.
[36] K. Tanaka, H. Kita, M. Okano, K. Okamoto, Polymer 33 (1992) 585–592.
[37] S.A. Stern, Y. Mi, H. Yamamoto, A.K. St Clair, J. Poly. Sci. B 27 (1989) 1887–1909.
[38] B. Seoane, C. Tellez, J. Coronas, C. Staudt, Sep Pur. Tech. 111 (2013) 72–81.
[39] T. Visser, G.H. Koops, M. Wessling, J Membr Sci. 252 (2005) 265–277.
[40] L. Ge, W. Zhou, V. Rudolph, Z. Zhu, J Mater. Chem. A 1 (2013) 6350–6358.
[41] M.B. Saeed, M.-S. Zhan, Eur Poly J. 42 (2006) 1844–1854.
[42] H.-T. Kim, S.-K. Kim, J.-K. Park, Poly. J. 31 (1999) 154–159.
[43] M. Kotera, T. Nishino, K. Nakamae, Polymer 41 (2000) 3615–3619.
[44] C.A. Pryde, J. Poly. Sci. Part A 27 (1989) 711–724.
[45] Y. Zhai, Q. Yang, R. Zhu, J. Mater Sci. 43 (2008) 338–344.
[46] E. Unsal, M. Cakmak, Polymer 55 (2014) 6569–6576.
[47] C. Joly, D.L. Cerf, C. Chappey, D. Langevin, G. Muller, Sep Pur. Tech. 16 (1997) 47–54.
[48] Y. Yang, P. Shukla, S. Wang, V. Rudolph, X.-M. Chen, Z. Zhu, RSC Adv. 3 (2013) 17065–17072.
[49] S. Basu, A. Cano-Odena, I.F.J. Vankelecom, Sep Pur Tech. 81 (2011) 31–40.
[50] J.L. Harding, M.M. Reynolds, J. Mater. Chem. B 2 (2014) 2530–2536.
[51] A.S. Khojin, S. Jana, W.H.K. Zong, J. Mater. Sci. 42 (2007) 6093–6101.
[52] H. Oh, PF. Green, Nat. Mater. 8 (2009) 139–143.
[53] B.P. Grady, A. Paul, J.E. Peters, W.T. Ford, Macromolecules 42 (2009) 6152–6158.
[54] K. Cho, D. Lee, M.S. Lee, C.E. Park, Polymer 38 (1997) 1615–1623.
[55] K.-S. Chang, C.-C. Hsiung, C.-C. Lin, K.-L. Tung, J. Phys. Chem. B 113 (2009) 10159–10169.
[56] Q. Yang, C. Zhong, J. Phys Chem B 110 (2006) 17776–17783.
[57] M.R. Coleman, W.J. Koros, J. Poly. Sci. B 32 (1994) 1915–1926.